A Practical Calibration Method for Stripe Laser Imaging System

Sooyeong Yi and Sungjae Min

***Abstract*—This paper presents a new practical calibration method of a stripe laser imaging system for the three-dimensional (3D) shape measurement of an object. The proposed calibration method has an integrated mathematical approach for the camera imaging parameters and the stripe laser light plane. A simple calibration block with checker board pattern attached is employed that has different inclination angle at each face. Because the same scene with the laser light on and off is used for the integrated calibration of the camera and the laser light plane, the calibration process is fast and efficient and the resultant calibration parameters are consistent. Experimental results demonstrated the performance of the proposed calibration method.**

***Index Terms*—3D shape measurement, camera parameter, calibration, stripe laser imaging, laser sweep plane**

I. Introduction

COMBINATION of an imaging camera and a laser scanner is generally used to acquire three-dimensional (3D) shape of an object [1-3]. The laser imaging system is a type of noncontact and active 3D measurement system that projects a collimated laser light of distinct frequency on a target object and measures the deformation of the laser light according to the shape of the object through a camera [4-6]. The 3D surface shape data can be calculated based on the triangulation.

Several studies have been conducted on the laser imaging system. A 3D scanning system was developed using a handheld linear laser light and a camera [7]. 3D point clouds of an object at different view angles with a variable field-of-view (FOV) camera were obtained by using stripe laser light image in [8]. An optical scanning mirror was used to improve the scanning speed of a laser triangulation sensor in [9]. A high-speed rotating optical diffuser was adopted to minimize the effects of geometrical fluctuations of the laser beam [10]. In [11], a calibration method of laser spot direction was proposed for a laser displacement sensor of an optical coordinate measuring system.

In some studies, structured light with a complex coded pattern was used instead of stripe laser light [12-14]. The line encoded structured light patterns were designed for surface measurement [15]. A calibration algorithms with some RGB features was proposed to calibrate the structured light patterns [16]. In [17], an overview of various pattern codification methods including space-, time-, and color-coding techniques was presented. A complex structured light pattern requires an expensive digital light processing projector [18,19]. Further progress and prospects of the structured light imaging methods for 3D data acquisition are available in [20-22]. A LiDAR sensor was combined with an imaging camera to obtain 3D data and the color information of an object simultaneously [23-25].

Because of the high measurement frequency and precision, the laser structured light imaging methods are applicable in various fields such as reverse engineering for industrial purposes [26], the restoration of cultural heritage [27,28], biomedical applications such as 3D dental measurement [29], human body shape measurement [30,31], the autonomous navigation of a mobile robot [32], the detection of surface crack in concrete [33] and object grasping with and auto-calibration of manipulator robots [35,36].

The coordinates of the stripe laser light and the camera imaging parameters should be known in advance to obtain metric reconstruction of target object's 3D shape by a laser imaging system. Herein, the camera imaging parameters implies the perspective transformation from the object coordinates to the camera image coordinates. Because there exist inevitable deviations between the nominal and the real coordinates caused by manufacturing and assembly tolerance, the real values should be obtained by calibration. Many approaches for the calibration have been studied over the years.

Most of the traditional stripe laser imaging systems had partitioned calibration steps for the camera imaging parameters and the laser light [7,16,37]. In [37], a calibration method for the laser plane equation was presented using a rectangular notch calibration block. The camera calibration was a prerequisite in the method and the notch block should be precisely aligned with the laser plane to obtain four laser image points for the laser calibration. On the other hand, an integrated calibration methods for both of the camera and laser light were presented in [38-41]. Four collinear triplet points on two orthogonal planes were used for the integrated calibration in [39], where an expensive equipment is required to acquire multiple calibration images on the orthogonal plane. In [40], a nonlinear calibration method was presented that accommodates the laser light and the imaging parameters as well as the radial distortion in the camera lens. Their approach requires an accurate linear motion table and time-consuming calibration image construction. An additional laser light was used for the calibration of a laser stripe imaging system mounted on a robot arm [41]. In the method, the camera imaging model was oversimplified and the additional laser should be precisely perpendicular to the first laser light.

The calibration methods for a laser imaging system based on the triangulation have the similar mathematical approaches in

This research was supported by the research program funded by National Research Foundation (Ministry of Education) of Korea (NRF-2018R1D1A1B07044841).

S. Yi and S. Min are with the department of Electrical and Information Engineering, Seoul National University of Science and Technology, Seoul 01811 Republic of Korea (e-mail: suylee@seoultech.ac.kr, msj5826@seoultech.ac.kr,).

general. In practical point of view, the calibration method is assessed by 1) the cost-effectiveness of the calibration equipment, 2) the integration of calibration steps for both of the stripe laser light and the camera imaging parameters and 3) the efficiency in calibration data acquisition. It is aimed in this paper to present a new practical calibration method for a stripe laser imaging system. The proposed method uses a simple calibration block with different inclination at each faces. The calibration block is easily produced by a commercially available tabletop 3D printer and a printed checker board pattern is attached in each face. The camera imaging parameters and the laser plane coefficients are obtained simultaneously from the same image of the calibration block acquired with the laser on and off. As the same image is used, the calibration procedure is simple and efficient and the resultant parameters are consistent. The rest of this paper is organized as follows: In Sec. II, a camera imaging model with the laser sweep plane of the laser imaging system is described. The proposed calibration method for the laser imaging system is presented in Sec. III. The experimental results and concluding remarks are presented in Sec. IV and Sec. V, respectively.

II. Modeling of Stripe Laser Imaging System

A. Camera Imaging System

Fig. 1 shows the transformations from the object coordinate system in the real world to the pixel coordinate system in the image sensor. Each of the transformations in the homogeneous representation is expressed as follows:

1) The geometric transformation between the object coordinates and the camera coordinates:

$$P_c = T_g \cdot P_w, \qquad T_g = \begin{bmatrix} R_{3\times3} & T_{3\times1} \\ 0_{3\times1} & 1 \end{bmatrix} \tag{1}$$

2) The perspective transformation from the camera coordinates to the image coordinates:

$$P_p = \frac{1}{z_c} T_p \cdot P_c, \quad T_p = \begin{bmatrix} f_x & 0 & c_x & 0 \\ 0 & f_y & c_y & 0 \\ 0 & 0 & 1 & 0 \end{bmatrix} \tag{2}$$

The symbols in (1) and (2) are summarized as follows:

- $P_w = \begin{bmatrix} x_w & y_w & z_w & 1 \end{bmatrix}^t$: A point in the object coordinate system

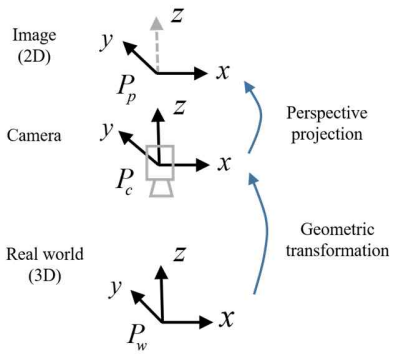

Fig. 1. Transformation of image coordinate system.

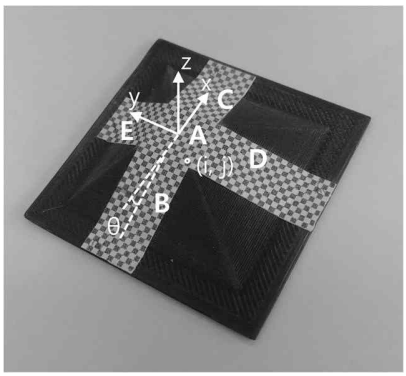

Fig. 2. Calibration block (photo).

- $P_c = \begin{bmatrix} x_c & y_c & z_c & 1 \end{bmatrix}^t$: A point in the camera coordinate system
- $P_p = \begin{bmatrix} x_p & y_p & 1 \end{bmatrix}^t$: A point in the image coordinate system
- T_g : The homogeneous transformation including rotation $R_{3\times3}$ and translation $T_{3\times1}$.
- $\left(f_x, f_y\right)$: The focal length of a camera lens.
- $\left(c_x, c_y\right)$: The optical axis of a camera lens.

The combination of (1) and (2) yields (3).

$$P_p = T_{3\times4} \cdot P_w \equiv \begin{bmatrix} x_p \\ y_p \\ 1 \end{bmatrix} = T_{3\times4} \cdot \begin{bmatrix} x_w \\ y_w \\ z_w \\ 1 \end{bmatrix} \tag{3}$$

where $T_{3\times4} = T_p \cdot T_g$. Eq. (3) is rewritten as (4),

$$\begin{bmatrix} x_p t_{31} - t_{11} & x_p t_{32} - t_{12} & x_p t_{33} - t_{13} & x_p t_{34} - t_{14} \\ y_p t_{31} - t_{21} & y_p t_{32} - t_{22} & y_p t_{33} - t_{23} & y_p t_{34} - t_{24} \\ 0 & 0 & 0 & 0 \end{bmatrix} \begin{bmatrix} x_w \\ y_w \\ z_w \\ 1 \end{bmatrix} = \mathbf{0} \tag{4}$$

where t_{ij}, $1 \le i \le 3$, $1 \le j \le 4$, represents the elements of the composite transformation $T_{3\times4}$.

B. Stripe Laser Sweep Plane

In the object coordinates, the stripe laser sweeps a plane that is represented as follows:

$$c_1 x_w + c_2 y_w + c_3 z_w + 1 = 0 \tag{5}$$

As a point on the laser stripe lies in the plane (5), this is an additional condition along with (4) for obtaining the 3D coordinate value $\left(x_w, y_w, z_w\right)$ of an object point. The combination of (4) and (5) yields (6) for computing the 3D coordinate value of an object point from the extracted laser pixel position $\left(x_p, y_p\right)$ in the image.

$$\begin{bmatrix} x_p t_{31}-t_{11} & x_p t_{32}-t_{12} & x_p t_{33}-t_{13} & x_p t_{34}-t_{14} \\ y_p t_{31}-t_{21} & y_p t_{32}-t_{22} & y_p t_{33}-t_{23} & y_p t_{34}-t_{24} \\ c_1 & c_2 & c_3 & 1 \end{bmatrix} \begin{bmatrix} x_w \\ y_w \\ z_w \\ 1 \end{bmatrix} = \mathbf{0}$$

$$\equiv \quad \begin{bmatrix} x_w \\ y_w \\ z_w \end{bmatrix} = \begin{bmatrix} x_p t_{31}-t_{11} & x_p t_{32}-t_{12} & x_p t_{33}-t_{13} \\ y_p t_{31}-t_{21} & y_p t_{32}-t_{22} & y_p t_{33}-t_{23} \\ c_1 & c_2 & c_3 \end{bmatrix}^{-1} \begin{bmatrix} -x_p t_{34}+t_{14} \\ -y_p t_{34}+t_{24} \\ -1 \end{bmatrix} \tag{6}$$

III. CALIBRATION

In this study, a calibration block with different inclinations at each face is employed to calibrate the parameters of the camera transformation and the coefficients of the laser sweep plane simultaneously. The calibration block can be produced with the appropriate precision by using a 3D printer. A printed checker board pattern is attached as shown in Fig. 2 to obtain a set of object points on the calibration block. In this study, the camera lens distortion is not considered because the distortion can be easily corrected by using the well-known camera calibration technique if necessary [42].

A. Calibration for t_{ij}, $1 \le i \le 3,\ 1 \le j \le 4$

The camera calibration algorithm proposed in [43] is briefly described here. Eq. (3) indicates that the vectors P_p and $T_{3\times4} \cdot P_w$ are collinear. Their vector product is $P_p \times (T \cdot P_w) = \mathbf{0}_{3\times1}$ and the expanded form is

$$\begin{bmatrix} \mathbf{0}_{4\times1}{}^t & -P_w{}^t & y_p P_w{}^t \\ P_w{}^t & \mathbf{0}_{4\times1}{}^t & -x_p P_w{}^t \\ -y_p P_w{}^t & x_p P_w{}^t & \mathbf{0}_{4\times1}{}^t \end{bmatrix} \begin{bmatrix} T_1{}^t \\ T_2{}^t \\ T_3{}^t \end{bmatrix} = \mathbf{0}_{3\times1} \tag{7}$$

where T_1, T_2, and T_3 represent the row vectors of $T_{3\times4}$. As (7) has only two independent conditions for the parameters in T_1, T_2, and T_3, the first two equations are selected to determine the parameters.

Given N pairs of image points and the corresponding 3D data in the object coordinates, $(P_{p1}, P_{w1}), \cdots, (P_{pN}, P_{wN})$, the following set of augmented equations is obtained:

$$\begin{bmatrix} \mathbf{0}^t & -P_{w1}{}^t & y_{p1} P_{w1}{}^t \\ P_{w1}{}^t & \mathbf{0}^t & -x_{p1} P_{w1}{}^t \\ \vdots & \vdots & \vdots \\ \mathbf{0}^t & -P_{wN}{}^t & y_{pN} P_{wN}{}^t \\ P_{wN}{}^t & \mathbf{0}^t & -x_{pN} P_{wN}{}^t \end{bmatrix} \begin{bmatrix} T_1{}^t \\ T_2{}^t \\ T_3{}^t \end{bmatrix} = \mathbf{0} \ \equiv \ \mathbf{A}_{2N\times12}\mathbf{T}_{12} = \mathbf{0} \tag{8}$$

The real coordinate values of the object points (grid points of the checker board pattern) can be obtained based on the known shape of the calibration block and the size of the printed grid. For example, $(x_{wij}, y_{wij}, z_{wij})$ on the face **B** shown in Fig. 2 is obtained as follows:

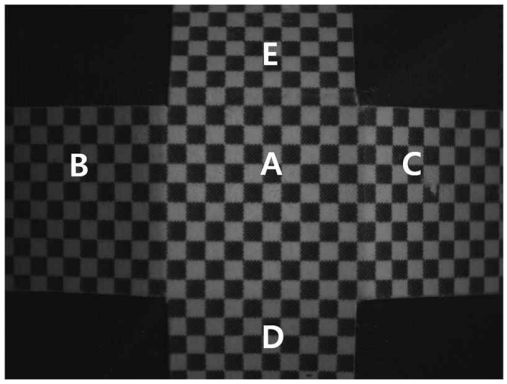

Fig. 3. Calibration block image with the laser off.

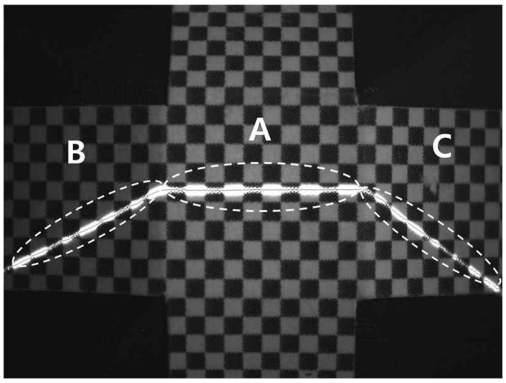

Fig. 4. Calibration block image with the laser on.

$$\begin{bmatrix} x_{wij} \\ y_{wij} \\ z_{wij} \end{bmatrix} = \begin{bmatrix} \cos(-\theta) & 0 & \sin(-\theta) \\ 0 & 1 & 0 \\ -\sin(-\theta) & 0 & \cos(-\theta) \end{bmatrix} \begin{bmatrix} \Delta_x \cdot i \\ \Delta_y \cdot j \\ 0 \end{bmatrix} + \begin{bmatrix} -5 \cdot \Delta_x \\ 0 \\ 0 \end{bmatrix} \tag{9}$$

where θ is the inclination angle of the face **B**, $\Delta_x (= \Delta_y)$ denotes the size of the grid, and (i, j) represents the index of a grid point on the face. It is assumed here that the coordinate frame is established at the center of the face **A** and the number of grids along x and y axes on the face **A** is 10 as shown in Fig. 2.

By matching each grid point in the experimental image in Fig. 3 with the coordinate value from (9), the calibration data sets (P_{pi}, P_{wi}) are obtained for (8). The number of the calibration data from the grid points in Fig. 3 is more than the number of unknown parameters in (8), which gives the overdetermined set of equations. The solution, $\hat{\mathbf{T}}$, of (8) is obtained using the well-known singular value decomposition as (10) :

$$\hat{\mathbf{T}} = \arg\min_{\mathbf{T}} \|\mathbf{A} \cdot \mathbf{T}\|, \qquad \|\mathbf{T}\| = 1 \tag{10}$$

B. Calibration for c_i, $1 \le i \le 3$

Fig. 4 shows the same calibration block image with the laser on. The dotted ellipses in Fig. 4 includes the sets of the extracted laser pixels (x_p, y_p) in the image. The coordinate values (x_w, y_w, z_w) corresponding to (x_p, y_p) can be computed by (4)

together with the plane equation of each face of the calibration block on which the laser pixels lie. For example, the real coordinate values (x_w, y_w, z_w) of the laser pixels on the face **B** in Fig. 4 can be obtained from (4) with the plane equation of **B** in (11).

$$z_w = \alpha x_w + \beta \tag{11}$$

where α and β are the known coefficients from the inclination angle of the calibration block. It is noted that the parameters for (4) was already obtained in (10). The same procedure is applied to the laser pixels on the faces, **A** and **C**. Consequently, a set of object points (x_w, y_w, z_w) on the laser sweep plane, (5) is obtained as follows:

$$\begin{bmatrix} x_{w1} & y_{w1} & z_{w1} \\ x_{w2} & y_{w2} & z_{w2} \\ \vdots & \vdots & \vdots \\ x_{wN} & y_{wN} & z_{wN} \end{bmatrix} \begin{bmatrix} c_1 \\ c_2 \\ c_3 \end{bmatrix} = -\mathbf{1} \quad \equiv \quad \mathbb{P}_w \mathbf{C} = -\mathbf{1} \tag{12}$$

where N denotes the number of object points corresponding to the laser pixels in the image and the vector **1** is an N-dimensional column vector with all the elements equal to 1. The solution of (12) is easily obtained using the pseudo-inverse as

$$\mathbf{C} = -\left(\mathbb{P}_w{}^t \mathbb{P}_w\right)^{-1} \mathbb{P}_w{}^t \mathbf{1} \tag{13}$$

IV. Experiments

A. Experimental setup

A schematic cross section of a laser imaging system is shown in Fig. 5. The effect of the slope angle of the laser sweep plane on the depth resolution is explained here. In $y-z$ section, the laser plane is represented by

$$z = \tan\phi \cdot (y - y_o) \tag{14}$$

where ϕ denotes the slope angle, f is the focal length of a camera, d represents the camera height and y_o is an object point on the laser sweep plane. The image position on the sensor plane is obtained by (15).

$$w = \frac{f \cdot y}{d - z} = \frac{f \cdot (\cot\phi \cdot z + y_o)}{d - z} \tag{15}$$

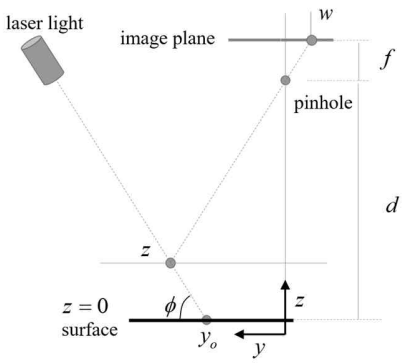

Fig. 5. Cross section of laser imaging system.

The depth resolution, (16), implies the displacement of an image point on the sensor plane according to change in the height of an object point:

$$\frac{dw}{dz} = \frac{f \cdot (d \cot\phi + y_o)}{d - z} \tag{16}$$

Eq. (16) shows that the depth resolution decreases monotonically according to ϕ, that is, the lower slope of the laser plane gives the higher measurement resolution in z-axis value of an object point. However, as the slope angle decrease, the image of the stripe laser light becomes thicker; it may cause the extraction error of the laser pixels in the image. The slope angle of the laser light is designed as around $\phi \approx 30^\circ$ by compromise in the experimental setup. Fig. 6 shows the laser light imaging system developed in this experiment. A stripe laser light of $660\,nm$ wavelength is used. The imaging system consists of a 2048×1536 resolution camera and a lens with 15° FOV that covers $30\,mm \times 30\,mm$ viewing range at $110\,mm$ height approximately. The lens with narrow FOV has negligible distortion in the image as shown in Fig. 3. Thus, the image correction is not considered in this experiment. The calibration block is illustrated in Fig 7, where b and h denote the bottom length and the height of each face, respectively. The inclination angles are calculated from b and h. The calibration block was easily produced by a commercial tabletop 3D printer with a nozzle of $0.4\,mm$ size. The step distance along the z-axis of the 3D printer is $0.08\,mm$. TABLE 1 shows the inclination angle of each face of the calibration block. A printed paper checker board pattern with the size $\Delta_x (= \Delta_y)$ of $1\,mm$ was attached on the calibration block as shown in Fig. 2.

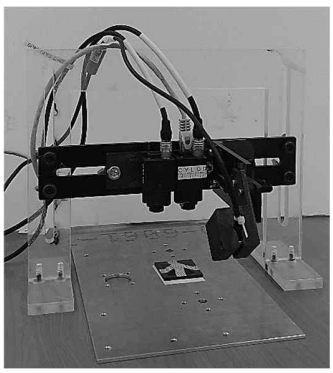

Fig. 6. Experimental laser light imaging system with a calibration block.

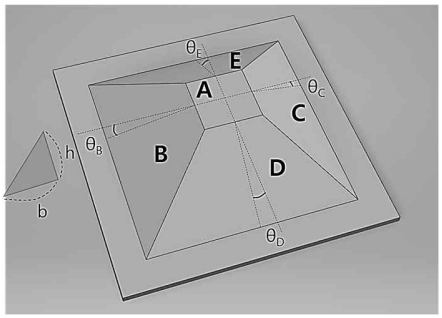

Fig. 7. Illustration of the calibration block.

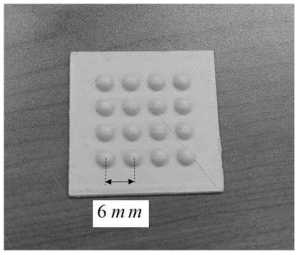

(a) Test object 1 (photo)

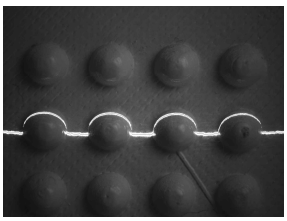

(b) Laser image

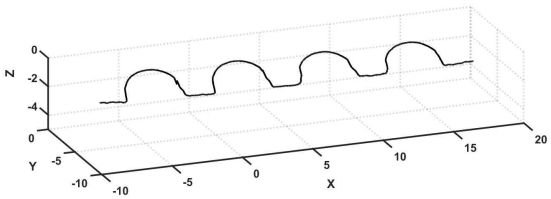

(c) 3D data reconstruction (one scan line)

Fig. 8. Experiment with test object 1.

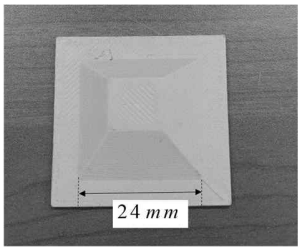

(a) Test object 2 (photo)

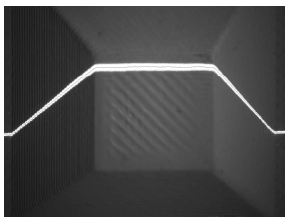

(b) Laser image

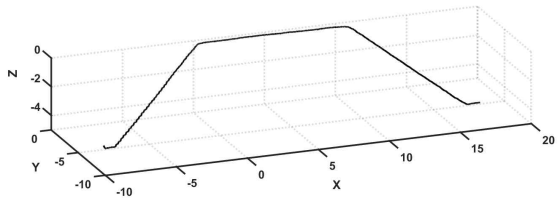

(c) 3D data reconstruction (one scan line)

Fig. 9. Experiment with test object 2.

TABLE I
SLOPE OF EACH FACE OF THE CALIBRATION BLOCK

Face	**A**	**B**	**C**	**D**	**E**
b (mm)	10.0	12.0	8.0	14.0	6.0
h (mm)	0.0	4.0	4.0	4.0	4.0
θ (deg.)	0.0	18.43	26.57	15.95	33.69

B. Result of calibration

• Imaging parameters, t_{ij}, $1 \le i \le 3,\ 1 \le j \le 4$

From the image in Fig. 3, it is possible to obtain the calibration data set, (P_{pi}, P_{wi}) that consists of the pixel position, (x_{pi}, y_{pi}) of each grid point in the image and the corresponding real 3D coordinate value, (x_{wi}, y_{wi}, z_{wi}) by using the known inclination angle with grid size of the calibration block. The following solution is obtained from (8) and (10) with the data set.

$$T_{3\times4} = \begin{bmatrix} -0.098814 & 0.000471 & 0.016820 & -0.844232 \\ -0.000302 & 0.101758 & 0.010458 & -0.516487 \\ 0.000000 & 0.000001 & 0.000016 & -0.001263 \end{bmatrix} \quad (17)$$

• Laser plane coefficients, c_i, $1 \le i \le 3$

The plane equation of the faces **A**, **B**, and **C** in the object coordinate system in Fig. 2 and Fig. 4 is represented by (18). There are 10×10 grids on the face **A** in Fig. 4.

$$\begin{cases} \text{Face } \mathbf{A}: & z_w = 0 \\ \text{Face } \mathbf{B}: & z_w = \tan(\theta_B)\, x_w - 5\Delta_x \\ \text{Face } \mathbf{C}: & z_w = -\tan(\theta_C)\, x_w + 5\Delta_x \end{cases} \quad (18)$$

Eq. (4) together with (18) determines (x_{wi}, y_{wi}, z_{wi}) from the laser pixel (x_{pi}, y_{pi}) on each face of the calibration block. As shown in Fig. 4, the laser light on a target object has several pixels with the maximum intensity in each column of the image. In this experiment, the laser pixel position is simply determined by the center of the uppermost and the lowermost pixel positions with the maximum intensity. As all the columns of the image in Fig. 4 have laser pixels, the number of object points (x_{wi}, y_{wi}, z_{wi}) corresponding to each extracted laser pixel is 2048. Using the data set of (x_{wi}, y_{wi}, z_{wi}), the solution for (12) was obtained from (13) as follows:

$$\mathbf{C} = \begin{bmatrix} -0.004648 & 0.226302 & -0.314155 \end{bmatrix}^t \quad (19)$$

C. Measurement result and 3D data reconstruction

The performance of 3D measurement in this study is investigated by using three test objects. The test object in Fig. 8 (a) is an array of hemispheres produced by the 3D printer. The height of the hemispheres is $2\,mm$. Fig. 8 (b) shows the experimental image with a laser scan line and Fig. 8 (c) is the result of the 3D reconstruction for the laser scan line.

Fig. 9 (a) shows the second test object, which has a similar shape as the calibration object used before but has a different size. The height of the test object 2 is $4\,mm$. Figs. 9 (b) and (c) shows the experimental image with a stripe laser light and the result of the 3D reconstruction.

Fig. 10 (a) is a test object stacked with twenty four A4 papers. Each A4 paper has $0.1\,mm$ thickness and the height of the object is $2.4\,mm$. In the experiment, the measurement along z-axis (depth) is the most relevant. As shown in Fig. 10 (b), each step in the stacked paper has around 10 pixels difference along y –axis in the image; it means the laser imaging system is capable of $0.01\,mm$ resolution in depth (z-axis) measurement. The results of measurement in z-axis are summarized in TABLE II. In the table, the standard deviations are obtained from ten repeated measurements. The measurement precision is within $0.05\,mm$ in the repeated experiment. The maximum measurement error is around $0.8\,mm$, which is deviated by 30% from the true value. It is possible to improve the accuracy by using the more accurate calibration block with the checker board pattern.

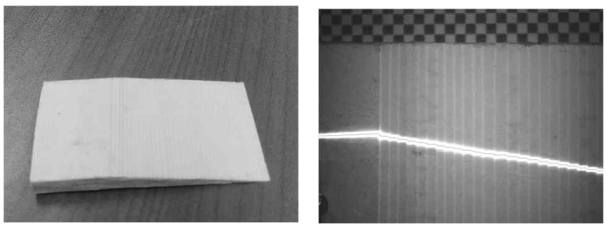

(a) Test object 3 (photo) (b) Laser image

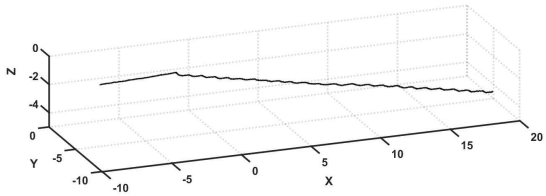

(c) 3D data reconstruction (one scan line)

Fig. 10. Experiment with test object 3.

As a summary, the proposed calibration method is compared with the some other methods in TABLE III. The aspects of the comparison are 1) the cost-effectiveness of the calibration equipment, 2) the integration of calibration steps for the stripe laser and the camera imaging parameters and 3) the efficiency in calibration data acquisition.

TABLE II
MEASUREMENT RESULTS

	Test object 1	Test object 2	Test object 3
True value (mm)	2.0	4.0	2.4
Measured average (mm)	2.64	4.47	3.16
Standard deviation (mm)	0.05	0.03	0.03
Repeatability (mm)	± 0.14	± 0.05	± 0.04

TABLE III
COMPARISON WITH OTHER CALIBRATION METHODS

	Calibration equipment	Integration of camera and laser calibration steps	Calibration data acquisition
[37]	Precise notch block	Partitioned calibrations	A laser image of notch block
[39]	Heavy metal frame with two orthogonal planes	Integrated calibration	Multiple images for stripe lights (not laser)
[40]	Calibration block on motion platform	Integrated calibration	Series of scanned images on motion platform
[41]	Additional laser light and gauge block	Partitioned calibrations	Several laser images of gauge block
Proposed	Calibration block with different inclination at face	Integrated calibration	An image with laser on and off

V. CONCLUSION

In this paper, a new practical calibration method was presented for a stripe laser imaging system. The proposed method used a calibration block with different inclination angle at each face. The calibration block can be easily produced using a tabletop 3D printer with proper precision. The imaging parameters and the laser sweep plane coefficients were obtained simultaneously by using the same calibration image with the laser on and off in the proposed method. Thus, the calibration process is simple and efficient and the resultant calibration parameters are consistent. The main advantages of the proposed calibration method are summarized as 1) consistency in the calibrated parameters because of the integrated calibration for the camera imaging parameters and the stripe laser, 2) cost-effectiveness of the calibration equipment and 3) efficiency in calibration data acquisition from a single calibration image with laser on and off. The experimental results demonstrated the performance of the proposed calibration method in terms of the 3D measurement precision up to tens of micrometers. The proposed calibration method is applicable to laser imaging systems for precise inspection, reverse engineering, or 3D shape reconstruction combined with the y -axis motion. It is possible to obtain the higher calibration accuracy by using a more accurate calibration block. Also, a pair of two stripe laser light can improve the measurement performance of a laser imaging system by reducing the shading area of a target object.

REFERENCES

[1] P. Payeur and C. Chen, "Registration of range measurements with compact surface representation," *IEEE Trans. Instrum. Meas.*, vol. 52, no. 5, pp. 1627–1634, Oct. 2003.
[2] L. Wei, C. Cappelle, and Y. Ruichek, "Camera/laser/GPS fusion method for vehicle positioning under extended NIS-based sensor validation," *IEEE Trans. Instrum. Meas.*, vol. 62, no. 11, pp. 3110–3122, Nov. 2013.
[3] A. Wan, J. Xu, D. Miao, and K. Chen, "An accurate point-based rigid registration method for laser tracker relocation," *IEEE Trans. Instrum. Meas.*, vol. 66, no. 2, pp. 254–262, Feb. 2017.
[4] J. Beraldin, F. Blais, L. Cournoyer, G. Godin, and M. Rioux, "Active 3D sensing," *NRC Technical Report 44159*, Ottawa, 2000.
[5] Z. Dong. X. Sun, W. Liu, and H. Yang, "Measurement of Free-Form Curved Surfaces Using Laser Triangulation," *Sensors*, 18, 3527, 2018.
[6] H. Khali, Y. Savaria, J. L. Houle, M. Rioux, J. A. Beraldin, and D. Poussart, "Improvement of sensor accuracy in the case of a variable surface reflectance gradient for active laser range finders," *IEEE Trans. Instrum. Meas.*, vol. 52, no. 6, pp. 1799–1808, Dec. 2003.
[7] Z. Zhang and L. Yuan, "Building a 3D scanner system based on monocular vision," *Applied Optics*, vol. 51, no. 11, pp. 1638-1644, 2012.
[8] J. Franca, M. Gazziro, A. Ide, and J. Saito, "A 3D scanning system based on laser triangulation and variable field of view", *IEEE Int'l Conf. on Image Processing*, 1, pp. 425-428, 2005.
[9] J. Schlarp, E. Csencsics, and G. Schitter, "Optical Scanning of a Laser Triangulation Sensor for 3-D Imaging," *IEEE Trans. Instrum. Meas.*, vol. 69, no. 6, June, 2020.
[10] C. Liu and S. Jiang, "A novel laser displacement sensor with improved robustness toward geometrical fluctuations of the laser beam," *Meas. Sci. Technol.*, vol. 24, no. 10, Aug. 2013, Art. no. 105101.
[11] B. Chao, L. Yong, F. Jian-guo, G. Xia, L. Lai-peng, and D. Pu, "Calibration of laser beam direction for optical coordinate measuring system," *Measurement*, vol. 73, pp. 191–199, Sep. 2015.
[12] A. Boyer and P. Payeur, "Enhancing Structured Light Range Imaging by Adaptation of Color, Exposure and Focus," *Proc. of IEEE Int'l Conf. on Computational Intelligence and Virtual Environments for Measurement Systems and Applications* (CIVEMSA), 2017.
[13] K. Liu, Y. Wang, D. Lau, Q. Hao, and L. Hassebrook, "Dual-frequency pattern scheme for high-speed 3-D shape measurement," *Optics Express*, vol. 18, no. 5, pp. 5229-5244 (2010)
[14] S. Tang, X. Zhang, Z. Song, L. Song, and H. Zeng, "Robust pattern decoding in shape-coded structured light," *Optics and Lasers in Engineering*, 96, pp. 50-62, 2017.

[15] R. Yang, S. Cheng, W. Yang, and Y. Chen, "Robust and accurate surface measurement using structured light," *IEEE Trans. Instrum. Meas.*, vol. 57, no. 6, pp. 1275–1280, Jun. 2008.
[16] Z. Feng, D. Man, and Z. Song, "A Pattern and Calibration Method for Single-Pattern Structured Light System," *IEEE Trans. Instrum. Meas.*, vol. 69, no. 6, June, 2020.
[17] J. Salvi, J. Pages, and J. Batlle, "Pattern codification strategies in structured light systems," *Pattern Recognition*, 37, pp. 827-849, 2004.
[18] O. Fleischmann and R. Koch, "Fast projector-camera calibration for interactive projection mapping," *Proc. of Int'l Conf. on Pattern Recognition* (ICPR), pp. 3798-3803, 2016.
[19] S. Zhang and P. Huang, "Novel method for structured light system calibration," *Optical Engineering*, vol. 45, no. 8, pp. 083601-083608, 2006.
[20] S. Zhang, "Recent progresses on real-time 3D shape measurement using digital fringe projection techniques," *Optics and Lasers in Engineering*, 48, pp. 149-158, 2010.
[21] S. Gorthi and P. Rastogi, "Fringe Projection Techniques: Whither we are?," *Optics and Lasers in Engineering*, vol. 48, no. 2, pp. 133-140, 2010.
[22] Y. Ko and S. Yi, "Development of Color 3D Scanner Using Laser Structured-light Imaging Method," *Current Optics and Photonics*, vol. 2, no. 6, pp. 554-562, 2018.
[23] Y. Zhuang, N. Jiang, H. Hu, and F. Yan, "3-D-laser-based scene measurement and place recognition for mobile robots in dynamic indoor environments," *IEEE Trans. Instrum. Meas.*, vol. 62, no. 2, pp. 438–450, Feb. 2013.
[24] Z. Hu, Y. Li, N. Li, and B. Zhao, "Extrinsic calibration of 2-D laser rangefinder and camera from single shot based on minimal solution," *IEEE Trans. Instrum. Meas.*, vol. 65, no. 4, pp. 915–929, Apr. 2016.
[25] S. Xie, D. Yang, K. Jiang, and Y. Zhong, "Pixels and 3-D points alignment method for the fusion of camera and LiDAR data," *IEEE Trans. Instrum. Meas.*, vol. 68, no. 10, pp. 3661-3676, Oct. 2019.
[26] F. Buonamici, M. Carfagni, and Y. Volpe, "Recent strategies for 3D reconstruction using Reverse Engineering: a bird's eye view," *Advances on Mechanics, Design Engineering and Manufacturing*, Lecture Notes in Mechanical Engineering, Springer, pp. 841-850, 2017.
[27] C. Rocchini, P. Cignoni, C. Montani, P. Pingi, and R. Scopigno, "A low cost 3D scanner based on structured light," *Computer Graphics Forum*, vol. 20, no. 3, pp. 299-308, 2001.
[28] G. Pavlidis, A. Koutsoudis, F. Arnaoutoglou, V. Tsioukas, and C. Chamzas, "Methods for 3D digitization of Cultural Heritage," *Jour. of Cultural Heritage*, 8, pp. 93-98, 2007.
[29] L. Chen and C. Huang, "Miniaturized 3D surface profilometer using digital fringe projection," *Measurement Science and Technology*, vol. 16, no. 5, pp. 1061-1068, 2005.
[30] J. Sturm, E. Bylow, F. Kahl, and D. Cremers, "CopyMe3D: Scanning and Printing Persons in 3D," *Proc. of German Conf. on Pattern Recognition*, pp. 405-414, 2013.
[31] F. Lilley, M. Lalor, and D. Burton, "Robust fringe analysis system for human body shape measurement," *Optical Engineering*, vol. 39, no. 1, pp. 187-195, 2000.
[32] J. Moigne and A. Waxman, "Structured light patterns for robot mobility," *IEEE Jour. of Robotics and Automation*, vol. 4, no. 5, pp. 541-548, 1988.
[33] P. Giri and S. Kharkovsky, "Detection of surface crack in concrete using measurement technique with laser displacement sensor," *IEEE Trans. Instrum. Meas.*, vol. 65, no. 8, pp. 1951–1953, Aug. 2016.
[34] J. Shen and N. Gans, "Robot-to-human feedback and automatic object grasping using an RGB-D camera–projector system," *Robotica*, Cambridge University Press, 2017.
[35] C. Wieghardt and B. Wagner, "Self-Calibration of a Mobile Manipulator Using Structured Light," *Proc. of IEEE Int'l Conf. on Advanced Robotics* (ICAR), pp. 197-203, 2017.
[36] M. Levoy, K. Pulli, B. Curless, S. Rusinkiewicz, D. Koller, L. Pereira, M. Ginzton, S. Anderson, J. Davis, J. Ginsberg, J. Shade, and D. Fulk, "The Digital Michelangelo Project: 3D Scanning of Large Statues," *Proc. of 27th annual conf. on Computer Graphics and Interactive Techniques* (SIGGRAPH'00), pp. 131-144, 2000.
[37] B. Abu-Nabah, A. ElSoussi, A. Alami, "Simple laser vision sensor calibration for surface profiling applications," *Optics and Lasers in Engineering*, 84, pp. 51-61, 2016.
[38] I. Reid, "Projective calibration of a laser-stripe range finder," Image and Vision Computing, vol. 14, pp. 659-666, 1996.
[39] D. Huynh, R. Owens and P. Hartmann, "Calibration of a structured light stripe system: a novel approach," Int'l Jour. of Computer Vision, vol. 33, pp. 73–86, 1999.
[40] A. Mclvor, "Nonlinear calibration of a laser stripe profiler," Optical Engineering, vol. 41, pp. 205–212, 2002.
[41] G. Idrobo-Pizo, J. Motta, and R. Sampaio, "A Calibration Method for a Laser Triangulation Scanner Mounted on a Robot Arm for Surface Mapping," *Sensors*, 19, 1783, 2019.
[42] Z. Zhang, "A flexible new technique for camera calibration," *IEEE Trans. Pattern Anal. Mach. Intell*. 22, pp. 1330–1334, 2000.
[43] D. Bertsekas, *Constrained Optimization and Lagrange Multiplier Methods*, Academic Press, New York, 2014.

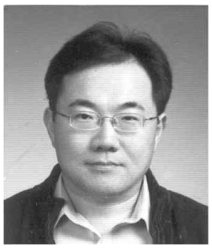

Sooyeong Yi received his M.S. and Ph.D. degrees in Electrical Engineering from Korea Advanced Institute of Science and Technology, in 1990 and 1994, respectively. During 1995-1999, he stayed in Human Robot Research Center in Korea Institute of Science and Technology as a senior researcher. He was a professor in the Division of Electronics and Information Engineering, Chonbuk National University, Korea from September 1999 to February 2007. He was also a post doctorial researcher in the Department of Computer Science, University of Southern California, Los Angeles in 1997 and a visiting researcher in the Dept. of Electrical and Computer Engineering, University of Illinois at Urbana-Champaign in 2005. He is now with the Department of Electrical and Information Engineering in Seoul National University of Technology, Korea. His primary research interest is in the area of robot vision, and intelligent control theory.

Sungjae Min was born in Seoul, Republic of Korea in 1998. He was a Researcher at Hands-on Technology, Korea from 2016 to 2017. Also, he participated in many robot competitions as the team leader of a robot club from 2014 to 2017. He is currently pursuing an academic degree in Electrical and Informational Engineering of Seoul National University of Science and Technology, Seoul, Korea. His research interests include humanoid robot, robot hand, robot vision, intelligent control, and mechatronics.